HHS Public Access

Author manuscript

Isr J Chem. Author manuscript; available in PMC 2017 October 01.

Published in final edited form as:

Isr J Chem. 2016 October ; 56(9-10): 649–659. doi:10.1002/ijch.201600016.

Activating Metal Sites for Biological Electron Transfer

Edward I. Solomon[a],*, **Ryan G. Hadt**[a],[b], and **Benjamin E.R. Snyder**[a]

[a]Department of Chemistry, Stanford University, Stanford, California 94305, United States

Abstract

This review focuses on the unique spectroscopic features of the blue copper active sites. These reflect a novel electronic structure that activates the site for rapid long-range electron transfer in its biological function. The role of the protein in determining the geometric and electronic structure of this site is defined, as is its contribution to function. This has been referred to as the entatic/rack-induced state. These concepts are then extended to cytochrome *c*, which is also determined to be in an entatic state.

Keywords

electron transfer; blue copper; cytochromes; structure-activity relationships; transition metal spectroscopy

1 - Introduction

There are three classes of metal active sites that participate in biological electron transfer (ET) (figure 1).[1a] In Cu chemistry, there is the mononuclear blue copper center with thiolate and thioether ligands, and the binuclear Cu_A site, with bridging thiolates and a thioether bound to one Cu center. In iron-sulfur biochemistry, there are the rubredoxins, ferredoxins, and HiPIP (high potential iron protein). These sites have different nuclearities, but all feature tetrahedral Fe coordinated by sulfur ligands, with Fe high spin in both redox states. Finally, in heme bioinorganic chemistry, there are the cytochromes – particularly cytochrome *c*, which binds Fe with a strong equatorial porphyrin ligand. Axial ligation is usually provided by imidazole and thioether ligands, which enforce a low spin Fe center in both redox states. These Cu and Fe sites have very different geometric and electronic structures covering a wide range of reduction potentials for their physiological function, but all satisfy two criteria required for efficient biological ET:[2] 1) there is minimal change in geometry with redox, resulting in a low reorganization energy λ in Marcus theory of ET; 2) there is efficient electronic coupling between the electron donor and acceptor, H_{DA}, over long distances through the protein.[3] This review focuses on how nature tunes the blue Cu site for efficient ET, and briefly extends these concepts to cytochrome *c* (cyt *c*).

Tel.: 650-723-9104 edward.solomon@stanford.edu.

[b]Current address: Chemical Sciences and Engineering Division, Argonne National Laboratory, Lemont, Illinois 60439, United States

2 – Unique Spectral Features of the Blue Copper Active Site

As shown in figure 2A, Cu(II) complexes normally have a tetragonal or square planar structure due to the Jahn-Teller effect. This leads to a highest energy ½-occupied $3d_{x2-y2}$ orbital. The high energy of this orbital reflects a strong σ-antibonding interaction with the ligands, as its lobes are oriented directly along the ligand-metal bonds. It should be emphasized that this is the redox active molecular orbital (RAMO) that plays the key role in function: long range ET. As predicted by Harry Gray and I,[4] the blue Cu site is tetrahedral (figure 2B) and this raised the idea that perhaps the protein opposes the Jahn-Teller distortion of the oxidized site, activating the Cu center for ET. The contribution of the protein in activating a metal site for function has been termed the entatic, or rack-induced state.[6] In addition to the distorted T_d structure, the blue Cu site has two interesting ligands: the aforementioned thiolate (of cysteine), with a short 2.1 Å S-Cu bond, and thioether (of methionine) with a long 2.9 Å S-Cu bond.[7]

Associated with the distorted T_d structure and unusual ligation are the unique spectral features of the blue Cu active sites.[8] In absorption spectroscopy, tetragonal and square planar Cu(II) complexes normally show d→d transitions from filled d orbitals to the ½-occupied $3d_{x2-y2}$ orbital. These are parity forbidden and thus weak (ε of ~40 $M^{-1}cm^{-1}$), and they appear at ~16000 cm^{-1} (600 nm) in the red spectral region (figure 2C). The blue Cu proteins have an extremely intense absorption band (ε of ~5000 $M^{-1}cm^{-1}$) in this region, however, resulting in their intense blue color. In EPR spectroscopy, normal Cu(II) complexes as in figure 2A exhibit a signal with a characteristically large 4 line splitting pattern (figure 2D, bottom) resulting from the hyperfine interaction of the electron spin in the $3d_{x2-y2}$ orbital with the nuclear spin of the Cu (I=3/2). In the blue Cu sites, the magnitude of this splitting is decreased by more than a factor of two (figure 2D, top).

Initially, these unique spectral features, in particular the small hyperfine splitting in EPR, were thought to derive from the distorted T_d structure mixing the Cu $4p_z$ orbital into the $3d_{x2-y2}$ ground state, which for straightforward reasons (i.e. its contribution to the spin dipolar coupling) would decrease the magnitude of A_{II}. We decided to experimentally evaluate this idea with Keith Hodgson and Britt Hedman by going up 10 orders of magnitude in photon energy, from the 10^{-4} cm^{-1} region of hyperfine coupling to the 9000 eV region of X-ray absorption spectroscopy at the Cu K edge.[9] As shown in figure 3A, at 8979 eV a core 1s electron is promoted to the RAMO of the blue Cu site. Since the s→d transition is electric dipole forbidden but s→p is electric dipole allowed, the intensity of this "pre-edge" transition should mostly reflect the Cu 4p mixing into the $3d_{x2-y2}$ orbital due to the distorted T_d ligand field of the blue Cu site. Figure 3B shows the X-ray absorption pre-edge of a powder of square planar $[CuCl_4]^{2-}$ and a frozen solution of the blue Cu protein plastocyanin. Note that the intensity of the 8979 eV feature greatly increases in the blue Cu site, indicating the presence of 4p mixing. To determine the nature of this mixing, we performed single crystal EPR studies of plastocyanin to determine that the electronic z axis is approximately along the long S(Met)-Cu bond,[10] and then analyzed polarized XAS data obtained with the electric field vector parallel and perpendicular to this z axis (figure 3C).[9] The dashed spectrum with E||z shows no pre-edge feature. This is the orientation that would show $4p_z$ mixing, and none is observed. All the pre-edge intensity is present in the E⊥z

XAS spectrum, reflecting $4p_{x,y}$ (and quadrupole)[11] character. This experiment eliminated the possibility that the small A_{II} reflects Cu $4p_z$ mixing, allowing us to focus instead on a highly covalent blue Cu active site. The idea is that covalency delocalizes the e^- spin onto the ligand, decreasing its interaction with the nuclear spin on the copper.[12]

The covalency of the Blue Cu site brings us to molecular orbital (MO) theory, and modern MO theory of transition metal sites often involves density function theory (DFT). At the top of table 1 and figure 4A are given results of two DFT calculations, one using a pure gga functional (BP86), and one with a hybrid functional having 20% Hartree-Fock mixing (B3LYP).[8] Both give very similar ground state wavefunctions for the blue Cu sites: a $3d_{x2-y2}$ orbital that is highly delocalized into the $p\pi$ orbital of the thiolate S. Quantitatively, however, they both give sites that are too covalent, with only 30% Cu(d) and 60% S(p) character. From experiment (*vide infra*) the blue Cu site has ~40% Cu(d) and ~40% S(p) in the ground state (table 1, middle). The calculations in figure 4A and the top of table 1 only contain the active site, however. Inclusion of the whole protein (bottom of table 1 and figure 4B) tunes down the covalency to a value close to experiment with 43% Cu(d) and 43% S(p). Inclusion of the protein contributes an H-bond to the thiolate S and carbonyl dipoles, which we have found change the covalency of the S(cys)-Cu bond.[13] This provides the protein a second coordination sphere mechanism to tune the reduction potential of the blue Cu site over ~200 mV for function, as decreasing the covalency preferentially destabilizes the oxidized state, increasing E^0.

3 – Definition of the Electronic Structure of the Blue Cu Site: New Spectroscopic Methods

We now focus on new methods we developed to experimentally determine the covalency of the Cu(II)-S(cys) bond (table 1, middle) and the π versus σ nature of the bonding interaction between the thiolate S and Cu(II) (figure 4A).

Cu L edge XAS was utilized (with Steve Cramer) to quantify the amount of $3d_{x2-y2}$ character in the RAMO of the blue Cu site.[14] From figure 5A, at 930 eV there is a Cu 2p→RAMO transition (the L_3 pre-edge). The 2p orbital is localized on the Cu, and p→d is electric dipole allowed. Therefore the intensity of the L_3 pre-edge quantifies the amount of $3d_{x2-y2}$ character in the RAMO ($(1-\alpha^2)$ in figure 5A). From figure 5B, the L_3 edge intensity is decreased for the blue Cu site in plastocyanin relative to square planar $[CuCl_4]^{2-}$, therefore there is less Cu(d) character in RAMO of the blue Cu site, reflecting its higher covalency. From a series of traditional spectroscopic studies of D_{4h} $[CuCl_4]^{2-}$, the ground state wavefunction has 61±2% $3d_{x2-y2}$ character.[15] Thus the intensity ratio of the blue Cu/ $[CuCl_4]^{2-}$ L edges quantifies the blue Cu site as having 41% Cu $3d_{x2-y2}$ character – a very covalent site that is tuned by the second coordination sphere of the protein (*vide supra*).

That this high covalency involved the thiolate S-Cu(II) bond came from ligand Kedge XAS,[9a] a method we developed with Keith Hodgson and Britt Hedman to directly experimentally define the amount of ligand character in all ½-occupied or unoccupied valence orbitals.[9a] From figure 6A, the sulfur K pre-edge is at 70 eV. This involves the S(1s)→RAMO transition. Since the 1s is localized on the sulfur and s→p is electric dipole

allowed, the intensity of this transition gives the cysteinate S contribution to the RAMO from covalent bonding (α^2 in figure 6A). From figure 6B, the blue Cu site in plastocyanin is ~2.5x as intense as tetb,[17] a thiolate-Cu(II) model with 14% S(p) character in its ground state. This demonstrates a key feature of the blue Cu site – a highly covalent Cu-S(cys) bond. It will be seen in the next section that this is also key to function.

The final spectroscopic method was the use of low temperature magnetic circular dichroism spectroscopy (LT MCD) to assign the unique Abs spectrum of the blue Cu site in order to define π and σ contributions to the covalency of the Cu(II)-S(cys) bond.[18,19] Figure 7A reproduces the Abs spectrum of blue Cu from figure 2C. Cooling to liquid He temperature sharpens the bands, and by correlating LT Abs with LT CD (not shown) and LT MCD (figure 7D), each method involving a different selection rule, there are 8 transitions required to fit the LT Abs spectrum in figure 7B. Band 4 is the characteristic intense Abs feature of the blue Cu center, while band 6 to lower energy also has some intensity. From our polarized single crystal absorption spectra of plastocyanin, both bands have the same polarization vector, one that correlates these bands with the Cu(II)-S(cys) bond.[10] At this point, one might assume a “normal” thiolate S to Cu charge transfer (CT) transition assignment (figure 7E, top), with a low-lying weak π CT and high energy intense σ CT. This reflects the fact that CT intensity is proportional to overlap of the donor and acceptor orbitals involved in the transition. As shown in figure 2A, for “normal” tetragonal Cu(II) complexes, the lobes of the $3d_{x2-y2}$ orbital are directed along ligand-metal bonds, maximizing σ overlap (figure 7E, top right). This “normal” CT assignment is not correct, however, as revealed by analysis of LT MCD (figure 7D) associated with the absorption bands (figure 7B). Bands 5–8 are all weak in Abs but intense in LT MCD. Based on the spin-orbit coupling mechanism required for LT MCD intensity, this requires that these transitions have mostly metal d character in the excited state, and thus are the four possible d→d transitions. Thus band 4, which is intense in Abs and weak in LT MCD, is the lowest energy π CT, while a higher energy weak transition is the S(pσ)→RAMO σ CT. Since CT intensity reflects orbital overlap, this inverted π/σ CT intensity pattern requires that the $3d_{x2-y2}$ orbital be rotated by 45° so its lobes bisect the Cu-S(Cys) bond (Fig 7E bottom right) reflecting the strong π bonding interaction of the thiolate with the Cu at the short 2.1 Å Cu-S(Cys) bond length.

These spectral methods show that the unique spectral features of the blue copper site reflect a *highly covalent thiolate-Cu(II) π bond*. In the next section we will see that this is key to function.

4 – Electronic Structure Contributions to Electron Transfer

Here the focus is on the electronic coupling matrix element for ET, H_{DA}. The multicopper oxidases (MCOs) provide an excellent system for this analysis, as the pathway for biological ET is clear. In the single blue copper proteins there are protein-protein docking issues in identifying the electron entry and exit pathways (although in the metallooxidases Fet3p and ceruloplasmin the Fe(II) binds tightly to its substrate binding site where one of its carboxylate ligands H-bonds to a His ligand of the blue copper, providing an electron entry pathway into this site).[20] In the MCOs, the thiolate ligand of the blue Cu site is flanked on either side in the sequence by imidazoles that ligate a trinuclear Cu cluster (Fig 8).[21a]

These enzymes function by taking an e^- from the substrate at the blue Cu site at the surface of the enzyme and transferring it rapidly (> 10^3 s^{-1}) over 13 Å to the trinuclear Cu cluster where O_2 is reduced to water (see [21b] for details of this mechanism). In Fig 8, the RAMO defined in the last section is superimposed on the blue Cu site. Qualitatively, it can be seen that the high anisotropic covalency of the Cu-S(**π**) bond activates the Cys-His pathway for rapid ET to the trinuclear Cu cluster.

Quantitatively we have evaluated H_{DA} for the Cys-His pathway of the multicopper oxidases in Fig 9A–D.[] The covalency of the Cu-S(Cys) bond has been varied by computationally changing the strength of an H-bond to its sulfur (Fig 9A). It is seen that H_{DA} increases linearly with the covalency of this bond. Equation 1 gives the rate of non-adiabatic ET:[2]

$$k_{ET} = \sqrt{\frac{4\pi}{h^2 \lambda k_b T}} |H_{DA}|^2 \exp\left(-\frac{(\Delta G^0 + \lambda)^2}{4\lambda k_b T}\right) \quad (1)$$

and is proportional to $(H_{DA})^2$. Thus the high covalency of the Cu-S(Cys) bond makes a major contribution to k_{ET}. Also from a detailed MO analysis of the superexchange pathways through the Cys-His link (figures 9B and 9D), it was found that one pathway (path 1, Fig. 9B) dominates H_{DA} in the multicopper oxidases. This superexchange pathway requires the **π** donor bonding of the thiolate sulfur (figure 9D) to propagate a hole through the valence orbitals of the Cys-His pathway to exit **σ** to the remote Cu of the TNC through a **π** to **σ** crossover in the molecular orbital interactions at the remote Cu (figure 9D and insert). Thus both the high covalency and the **π** nature of the Cu-S(Cys) bond (responsible for its unique spectroscopic features) are critical to the effective ET of the blue Cu site. In the next section we consider the role of the protein in determining this electronic structure.

5 – Role of the Protein in Active Site Geometric and Electronic Structure: the Entatic/Rack Induced State

In figure 10 we consider a series of sites related to blue Cu, all with the same Cys/Met/2His ligand sets. These range in color from the blue of plastocyanin to green in nitrite reductase (NiR). As shown in figure 10A, this color change reflects a change in the thiolate-Cu bond from **π** donor in the blue Cu site in plastocyanin (the intense low energy **π** and weak high energy **σ** CT) to **σ** donor in the green site in nitrite reductase (weak **π**, intense **σ** CT at higher energy, hence the green color). From Fig 10B this change in electronic structure reflects a change in geometric structure: in going from the blue to green copper site, the thioether bond contracts 0.3 Å, the thiolate bond elongates by 0.1 Å, and the S(Met)-Cu-S(Cys) plane rotates into the N(His)-Cu-N(His) plane, a Jahn-Teller distortion toward a more tetragonal structure. Clearly, the protein influences the geometric and electronic structure of these blue Cu related active sites. The structural correlation in figure 10B suggested the thioether(S)-Cu bonding interaction determines this distortion. To evaluate this possibility, the green Cu site in nitrite reductase, which has the strongest Met(S)-Cu bond at 2.5 Å, was mutated (with Charles Scholes) to replace the methionine with a non-coordinating threonine.[23b] As shown in Fig 11A, this green copper variant now expresses a blue copper

site. Thus the thioether coordination by the protein controls the geometric and electronic structure of the blue Cu site.

Insight into the role of the thioether ligand in function came from further studies on the green copper site in nitrite reductase.[24] From Fig 11B this green site is present in a thermodynamic equilibrium with a blue Cu site. At low temperature only the green site is present. This is therefore the enthalpically favored form. Increasing the temperature converts the green Cu into a blue Cu site - the entropically favored form. From resonance Raman studies into both the σ CT of the green site and the π CT of the blue site in Fig 11B, the blue/green transition is associated with loss of the thioether ligand at elevated temperatures. We used the temperature dependence of the conversion to obtain an experimental value for the strength of the thioether-Cu(II) bond, ΔH = 5 kcal/mol. This was reproduced with electronic structure calculations, which were further used to estimate the strength of the thioether-Cu(I) bond in the reduced state, ΔH = 1 kcal/mol (figure 11C). Thus the thioether-Cu bond is very weak in both redox states (partially due to compensation by thiolate donation), but preferentially for the reduced site. This provides important insight into the role of the protein in function, i.e. the nature of the entatic/rack state in the blue copper proteins. The protein keeps the thioether bound to the Cu at physiological temperatures, opposing the entropic contribution to the Gibbs free energy. The increased thioether-metal bond strength for Cu(II) relative to Cu(I) stabilizes the oxidized over the reduced state, proving a first coordination sphere mechanism for the protein to tune down the reduction potential by up to 200 mV for function. Parallel studies were done on the binuclear Cu_A center in Fig 1, which defined an equivalent role of the protein stabilized thioether-Cu bond: to stabilize the oxidized over the reduced state, and to tune down the Cu_A reduction potential.[25] From Fig 1, cytochrome c has a thioether-metal bond that was thought to play the opposite role in function. This is considered in the next section.

6 – Nature of the Fe-S(Met) Bond in Cytochrome *c*

The literature on cytochrome *c* (cyt *c*) has generally considered the axial methionine to bind more strongly to the reduced rather than the oxidized site, i.e., ΔH Fe(II)-S(Met) > ΔH Fe(III)-S(Met).[26] This was thought to tune the reduction potential up by ~200 meV. This increased potential was key to the seminal studies of Gray and Winkler, which used photoinduced ET to trigger protein folding, and elucidated the folding process for the first time on fast time-scales.[26h,i]

We wanted to experimentally probe the covalency of the Met(S)-Fe bond. S Kedge XAS could not be used since the effective nuclear charge on the sulfur in methionine is higher than in the thiolate, which shifts the pre-edge (as in Fig 6) into the edge. L-edge XAS could be used (Fig 12A), where for Fe there can be e^- holes in both the dπ and dσ orbitals. Thus differential orbital covalency (DOC) can be experimentally measured.[27] However, L-edge XAS is not appropriate for metalloprotein solutions (as in trapped enzyme intermediates) due to experimental conditions (e.g., UHV, e^- yield detection, etc.). Thus excitation into the K-edge (appropriate experimental conditions for frozen enzyme intermediates) was used to obtain the L-edge using resonant inelastic X-ray scattering, 1s2p RIXS.[28] As shown in Fig 12B, the experiment involves 1s→3d excitation coupled to 2p→1s emission to fill the 1s

core hole. This produces the same final state as in L-edge XAS but through the resonance process. The experiment produces the 1s2p RIXS planes in Fig 12C where the x-axis scans the excitation energy and the y-axis scans the energy difference to the 2p → 1s emission. Vertical cuts through these RIXS planes produce the “L-edge like” spectra in Fig 12D. These were obtained for cyt c (solid lines) and a bis-imidazole reference complex (dashed lines). The data shown in Fig 12D are for the ferric sites where both π (green) and σ (red) covalencies could be separately obtained through the proper vertical cuts in Fig 12C. 1s2p RIXS experiments were also done on the ferrous sites. From these 1s2p RIXS data it was experimentally determined that the Fe(III)-SMet bond is, in fact, more covalent than the Fe(II)-S(Met) bond. This was reproduced with DFT calculations, which further showed (Table 2) that the thioether(S)-Fe(III) bond is in fact stronger than the thioether(S)-Fe(II) bond. This is the same behavior as in the blue copper[24] and Cu_A[25] active sites. However, the 1s2p RIXS experiments and calculations further showed that the Im(N)-Fe(III) bond was even stronger than the Im(N)-Fe(II) bond (relative to the thioether), and from the calculations, this is also the case for H_2O, binding more strongly to the Fe(III) than the Fe(II) (than the thioether). Thus the thioether does in fact increase the reduction potential of cyt c, but this is relative to the ligand that replaces it in solution (Table 2). Table 2 further shows that the thioether-Fe bond is also very weak, particularly for the reduced site, and should also be considered as in an entatic/rack induced state, keeping the thioether bound to the Fe at physiological temperatures.[28]

7 – Summary and Outlook

In bioinorganic chemistry, metalloproteins often exhibit unique spectroscopic features reflecting novel geometric and electronic structures that make significant contributions to function. For the blue copper site, the intense absorption band at ~16000 cm^{-1} and low hyperfine coupling of the electron spin to the nuclear spin on the Cu both reflect the highly covalent Cu-S_{cys} π bond. Further for blue copper sites, the role of the protein in imposing active site structure (i.e. the entatic/rack-induced state) has been defined (i.e. keeping the thioether bound at physiological temperature to tune down the reduction potential) and extended to the binuclear Cu_A center and to cytochrome *c*. For cytochrome *c*, we are now pursuing ultrafast laser experiments to heat the heme by > 300 K and monitor the effect on the thioether(S)-Fe(II) bond (through Fe Kβ emission and X-ray absorption near edge spectra) using the X-ray free-electron laser at SLAC to quantify its bond strength in the protein relative to the unconstrained calculations in table 2.

Concluding Comment

On the occasion of Harry Gray’s 80th birthday, Ed Solomon would like to take this opportunity to thank Harry for bringing him into a field where you can pursue rigorous spectroscopy on amazing molecules, and where the insights you derive have great impact on many areas of science.

Acknowledgments

This work was supported by a grant from the NIH (DK31450 to E.I.S.).

References

1. a) Liu J, Chakraborty S, Hosseinzadeh P, Yu Y, Tian S, Petrik I, Bhagi A, Lu Y. Chemical Reviews. 2014; 114:4366–4469. [PubMed: 24758379] b) Solomon EI. Inorg Chem. 2006; 45:8012–8025. [PubMed: 16999398]
2. Marcus S. Biochim Biophys Acta. 1985; 811:265.
3. a) Newton MD. Chem Rev. 1991; 91:767.b) Levich VG, Dogonadze R. Dokl Acad Nauk. 1960; 133:159–161.
4. Solomon EI, Hare JW, Gray HB. Proc Natl Acad Sci. 1976; 73:1389. [PubMed: 818636]
5. Colman PM, Freeman HC, Guss JM, Murata M, Norris VA, Ramshaw JAM, Venkatappa MP. Nature. 1978; 272:319–324.
6. a) Williams RJP. Eur J Biochem. 1995; 234:363. [PubMed: 8536678] b) Malmström BG. Eur J Biochem. 1994; 223:711. [PubMed: 8055947] c) Gray HB, Malmström BG, Williams RJP. J Biol Inorg Chem. 2000; 5:551. [PubMed: 11085645]
7. a) Guss JM, Freeman HC. J Mol Biol. 1983; 169:521. [PubMed: 6620385] b) Guss JM, Bartunik HD, Freeman HC. Acta Crystallogr B. 1992; B48:790.
8. Solomon EI, Szilagyi RK, DeBeer GS, Basumallick L. Chem Rev. 2004; 104:419. [PubMed: 14871131]
9. a) Shadle SE, Penner-Hahn JE, Schugar HJ, Hedman B, Hodgson KO, Solomon EI. J Am Chem Soc. 1993; 115:767.b) Scott RA, Hahn JE, Doniach S, Freeman HC, Hodgson KO. J Am Chem Soc. 1982; 104:5364.
10. Penfield KW, Gay RR, Himmelwright RS, Eickman NC, Freeman HC, Solomon EI. J Am Chem Soc. 1981; 103:4382.
11. Hahn JE, Scott RA, Hodgson KO, Doniach S, Desjardins SR, Solomon EI. Chem Phys Lett. 1982; 88:595–598.
12. Penfield KW, Gewirth AA, Solomon EI. J Am Chem Soc. 1985; 107:4519.
13. Hadt RG, Sun N, Marshall NM, Hodgson KO, Hedman B, Lu Y, Solomon EI. J Am Chem Soc. 2012; 134:16701. [PubMed: 22985400]
14. George SJ, Lowery MD, Solomon EI, Cramer SP. J Am Chem Soc. 1993; 115:2968.
15. Didziulis SV, Cohen SL, Gewirth AA, Solomon EI. J Am Chem Soc. 1988; 110:250–268.
16. Hedman B, Hodgson KO, Solomon EI. J Am Chem Soc. 1990; 112:1643–1645.
17. Hughley JL, Fawcett TG, Rudich SM, Lalancette RA, Potenza JA, Schugar HJ. J Am Chem Soc. 1979; 101:2617.
18. Gewirth AA, Solomon EI. J Am Chem Soc. 1988; 110:3811–3819.
19. Solomon EI, Baldwin MJ, Lowery MD. Chem Rev. 1992; 92:521.
20. Quintanar L, Gebhard MS, Wang T-P, Kosman DJ, Solomon EI. J Am Chem Soc. 2004; 126:6579. [PubMed: 15161286]
21. a) Messerschmidt A, Rossi A, Ladenstein R, Huber R, Bolognesi M, Gatti G, Marchesini A, Petruzzelli R, Finazzi-Agró A. J Mol Bio. 1989; 206:513–529. [PubMed: 2716059] b) Solomon EI, Heppner DE, Johnston EM, Ginsbach JW, Cirera J, Qayyum M, Kieber-Emmons MT, Kjaergaard CH, Hadt RG, Tian L. Chem Rev. 2014; 114:3659. [PubMed: 24588098]
22. Hadt RG, Gorelsky SI, Solomon EI. J Am Chem Soc. 2014; 136:15034. [PubMed: 25310460]
23. a) LaCroix LB, Randall DW, Nersissian AM, Hoitink CW, Canters GW, Valentine JS, Solomon EI. J Am Chem Soc. 1998; 120:9621–9631.b) Basumallick L, Szilagyi RK, Zhao Y, Shapleigh JP, Scholes CP, Solomon EI. J Am Chem Soc. 2003; 125:14784. [PubMed: 14640653]
24. Ghosh S, Xie X, Dey A, Sun Y, Scholes CP, Solomon EI. Proc Natl Acad Sci. 2009; 106:4969. [PubMed: 19282479]
25. Tsai M-L, Hadt RG, Marshall NM, Wilson TD, Lu Y, Solomon EI. Proc Natl Acad Sci. 2013; 110:14658. [PubMed: 23964128]
26. a) Raphael AL, Gray HB. Proteins: Struct, Funct, Bioinf. 1989; 6:338.b) Ye T, Kaur R, Senguen FT, Michel LV, Bren KL, Elliott SJ. J Am Chem Soc. 2009; 130:6682.c) Hantgan RR, Taniuchi H. J Biol Chem. 1978; 253:5373. [PubMed: 209037] d) Schejter A, Plotkin B. J Biol Chem. 1988; 255:353.e) Tezcan FA, Winkler JR, Gray HB. J Am Chem Soc. 1998; 120:13383–13388.f) Vashi

PR, Marques HM. J Inorg Biochem. 2004; 98:1471–1482. [PubMed: 15337599] g) Lushington GH, Cowley AB, Silchenko S, Lukat-Rodgers GS, Rodgers KR, Benson DR. Inorg Chem. 2003; 42:7550–7559. [PubMed: 14606851] h) Pascher T, Chesick JP, Winkler JR, Gray HB. Science. 1996; 271:1558–1560. [PubMed: 8599112] i) Mines GA, Pascher T, Lee SC, Winkler JR, Gray HB. Chem Biol. 1996; 3:491–497. [PubMed: 8807879] j) Cohen DS, Pielak GJ. J Am Chem Soc. 1995; 117:1675.k) Cheng MC, Rich AM, Armstrong RS, Ellis PJ, Lay PA. Inorg Chem. 1999; 38:5703.

27. Wasinger EC, de Groot FM, Hedman B, Hodgson KO, Solomon EI. J Am Chem Soc. 2003; 125:12894–12906. [PubMed: 14558838]
28. Kroll T, Hadt RG, Wilson SA, Lundberg M, Yan JJ, Weng TC, Sokaras D, Alonso-Mori R, Casa D, Upton MH, Hedman B, Hodgson KO, Solomon EI. J Am Chem Soc. 2014; 136:18087. [PubMed: 25475739]

Biographies

Edward I. Solomon received his Ph.D. at Princeton (1972) and was a postdoctoral fellow at the Ørsted institute in Denmark and at Caltech. He started his career at MIT in 1975, became full professor in 1981, and then joined the faculty at Stanford in 1982 where he is now the Monroe E. Spaght Professor of Humanities and Sciences and Professor of Photon Science at SLAC National Accelerator Laboratory. Professor Solomon's research in the fields of physical-inorganic and bioinorganic chemistry has significantly advanced our understanding of metal sites involved in electron and oxo atom transfer, O_2 binding, activation and reduction to water by copper proteins, and structure/function correlations over non-heme iron enzymes.

Ryan G. Hadt Ryan G. Hadt received his B.S. and M.S. degrees in chemistry from the University of Minnesota Duluth (with V. N. Nemykin) and completed his Ph.D. at Stanford University (with E. I. Solomon). He was a visiting postdoctoral fellow at Harvard University (with D. G. Nocera) before continuing research at Argonne National Laboratory (with L. X. Chen), where he has recently accepted the Enrico Fermi Fellowship. Much of his research is focused on understanding ground and excited state electronic structure contributions to transition metal catalysis and photochemistry, employing a wide range of steady state and time-resolved spectroscopies.

Benjamin E.R. Snyder received a B.S. in chemistry and a B.A. in mathematics from the University of Rochester in 2012. He is now an NSF fellow pursuing his Ph.D. in physical inorganic chemistry at Stanford University under the supervision of Prof. Edward Solomon. His research focuses on spectroscopic and computational elucidation of Cu and Fe active sites in zeolites, their activation for selective hydrocarbon oxidation, and how this relates to analogous Cu and Fe active sites in biology.

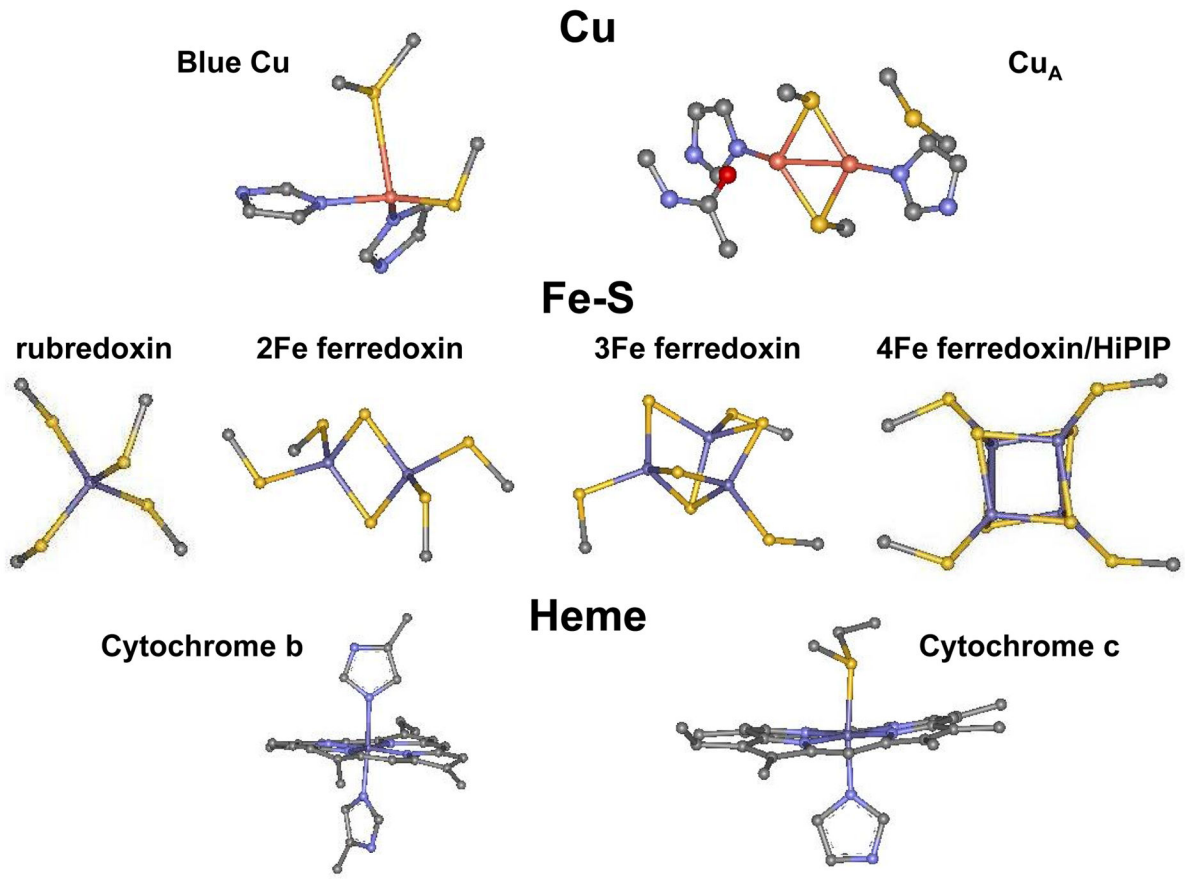

Figure 1.

Cu and Fe active sites in biological electron transfer. Adapted with permission from [1b]. Copyright 1996, American Chemical Society.

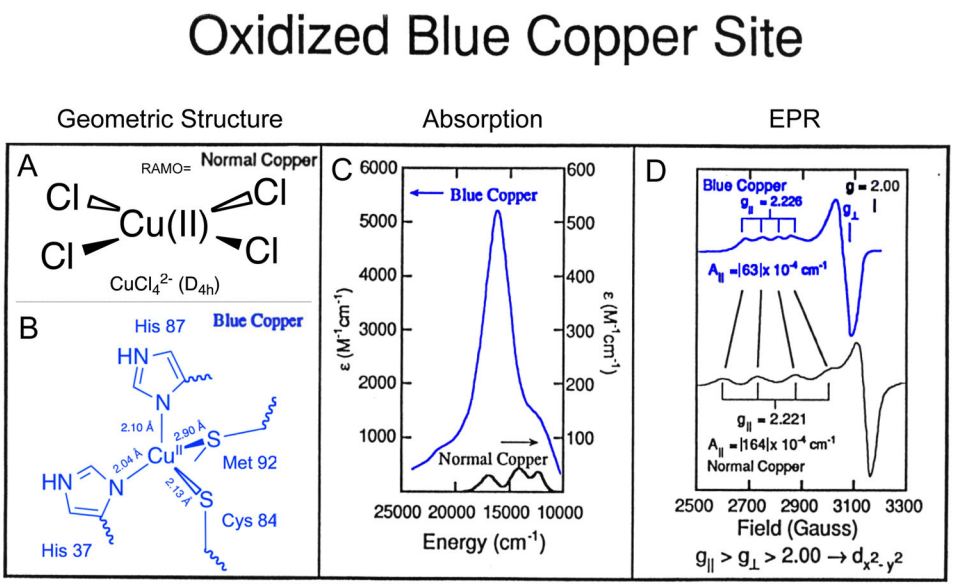

Figure 2.

Comparison of the (A,B) geometric structure,[5] (C) absorption spectra, and (D) EPR spectra of D_{4h} $[CuCl_4]^{2-}$ (normal Cu) and blue Cu.

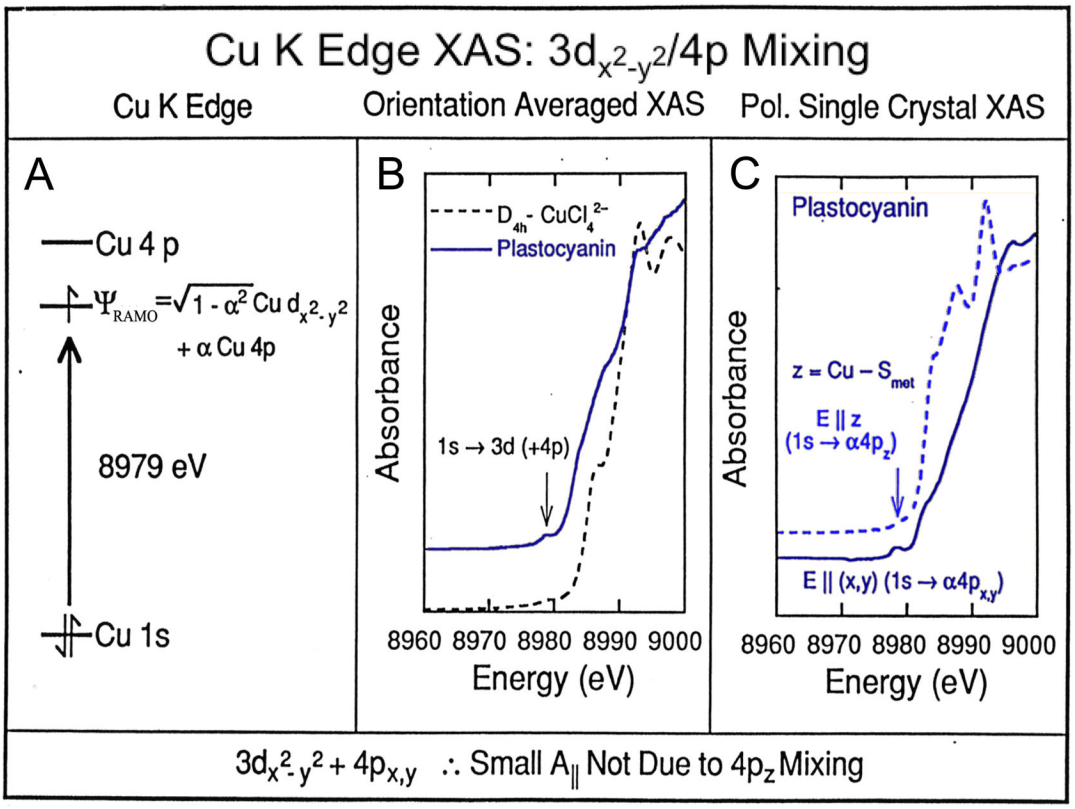

Figure 3.

(A) The pre-edge transition in Cu K-edge X-ray absorption spectroscopy. (B) Comparison of Cu K-edge spectra from D_{4h} $[CuCl4]^{2-}$ (normal Cu) and plastocyanin (a blue Cu protein). (C) Single crystal polarized XAS data from plastocyanin collected with the E vector parallel (blue) and perpendicular (purple) to the *z* axis defined from single crystal EPR. Adapted with permission from [8]. Copyright 2004, American Chemical Society.

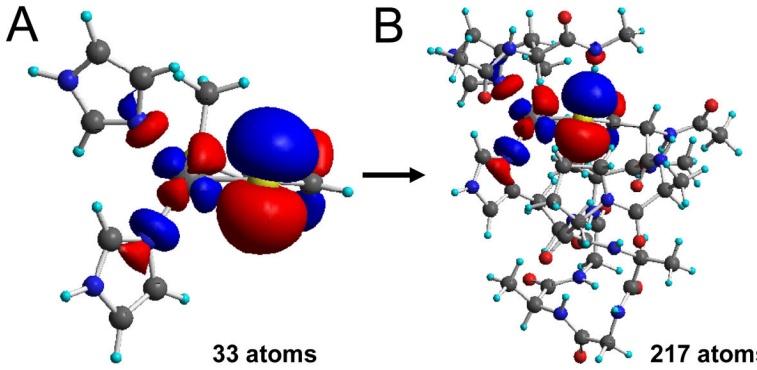

Figure 4.

(A) Small and (B) large DFT models of the blue Cu active site, showing the contour of the RAMO. Adapted with permission from [1b]. Copyright 2006, American Chemical Society.

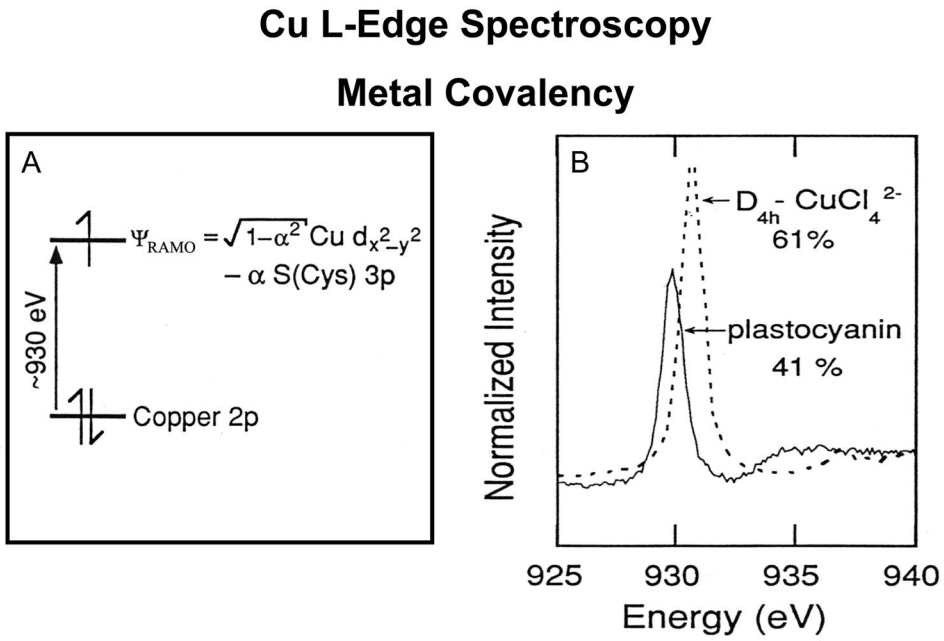

Figure 5.

(A) The L edge transition in Cu XAS. (B) Comparison of L_3 edge intensities of D_{4h} $[CuCl_4]^{2-}$ (normal Cu) and plastocyanin (blue Cu). Adapted with permission from [8]. Copyright 2004, American Chemical Society.

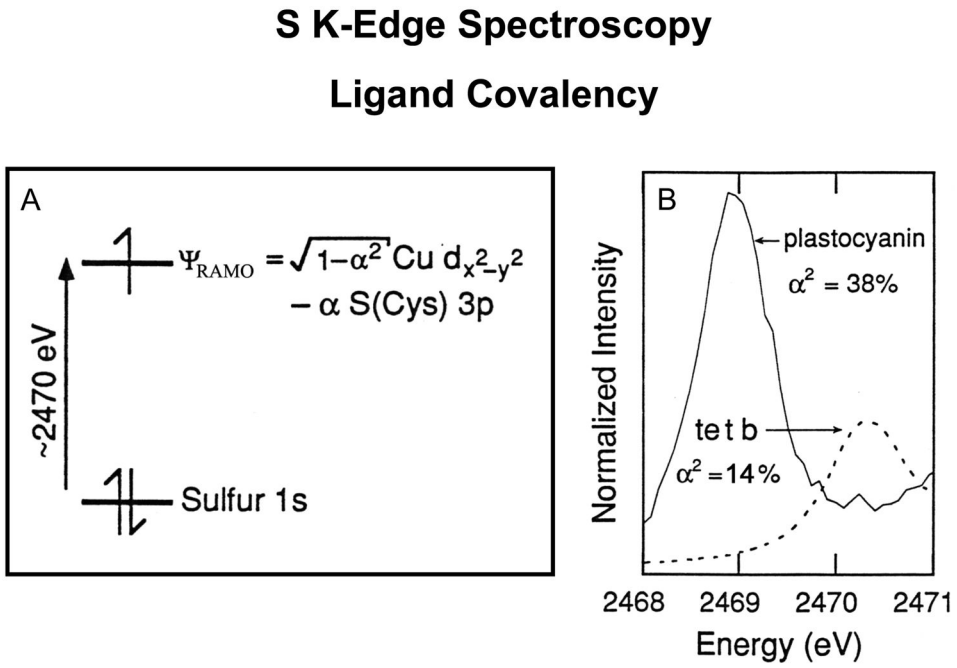

Figure 6.

(A) The pre-edge transition in S K edge XAS. (B) Comparison of pre-edge intensities of tetb (normal Cu/S model) and plastocyanin (blue Cu). Adapted with permission from [8]. Copyright 2004, American Chemical Society.

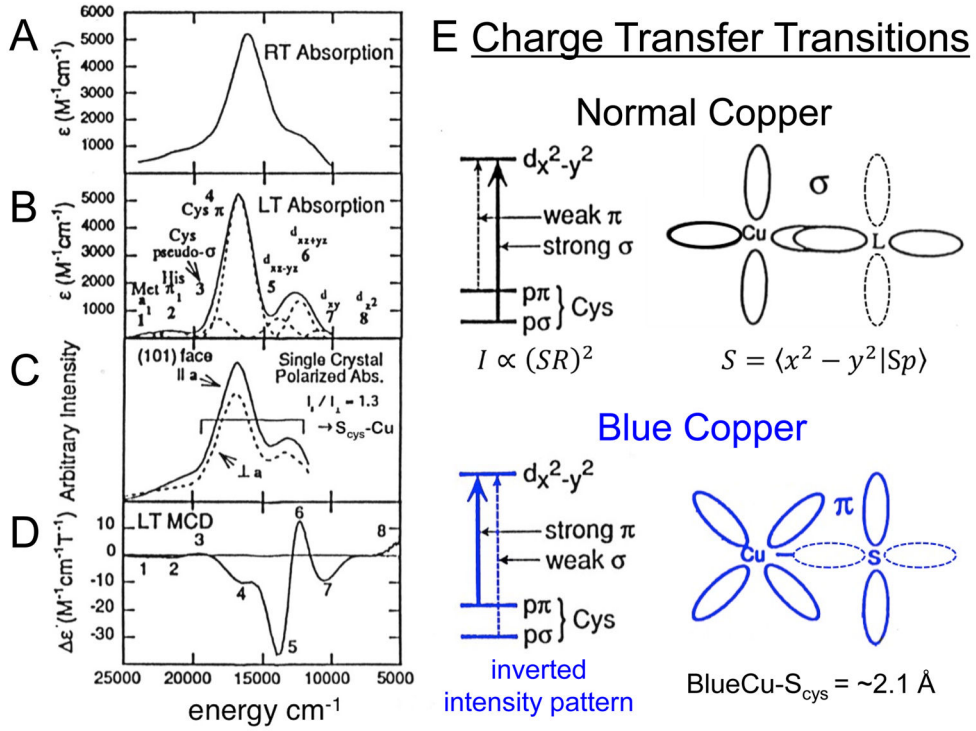

Figure 7.

Correlation of (A) RT Abs, (B) LT Abs, (C) single crystal polarized Abs, and (D) LT MCD spectral data for the blue Cu protein plastocyanin. (E) Comparison of σ and π charge transfer intensity for normal Cu (top) and blue Cu (bottom).

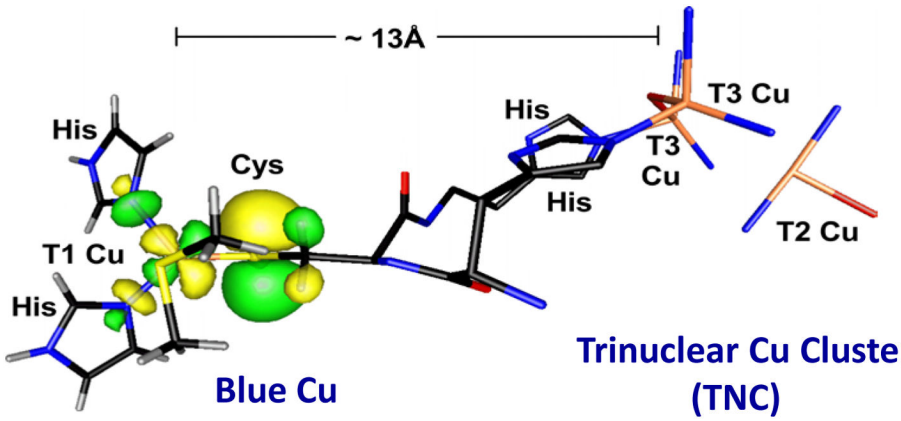

Figure 8.

Active site of a multi-copper oxidase, showing the blue Cu and trinuclear Cu sites separated by ~13 Å but connected by a Cys-His pathway. The RAMO of the blue Cu site is superimposed. Adapted with permission from [1b]. Copyright 2006, American Chemical Society.

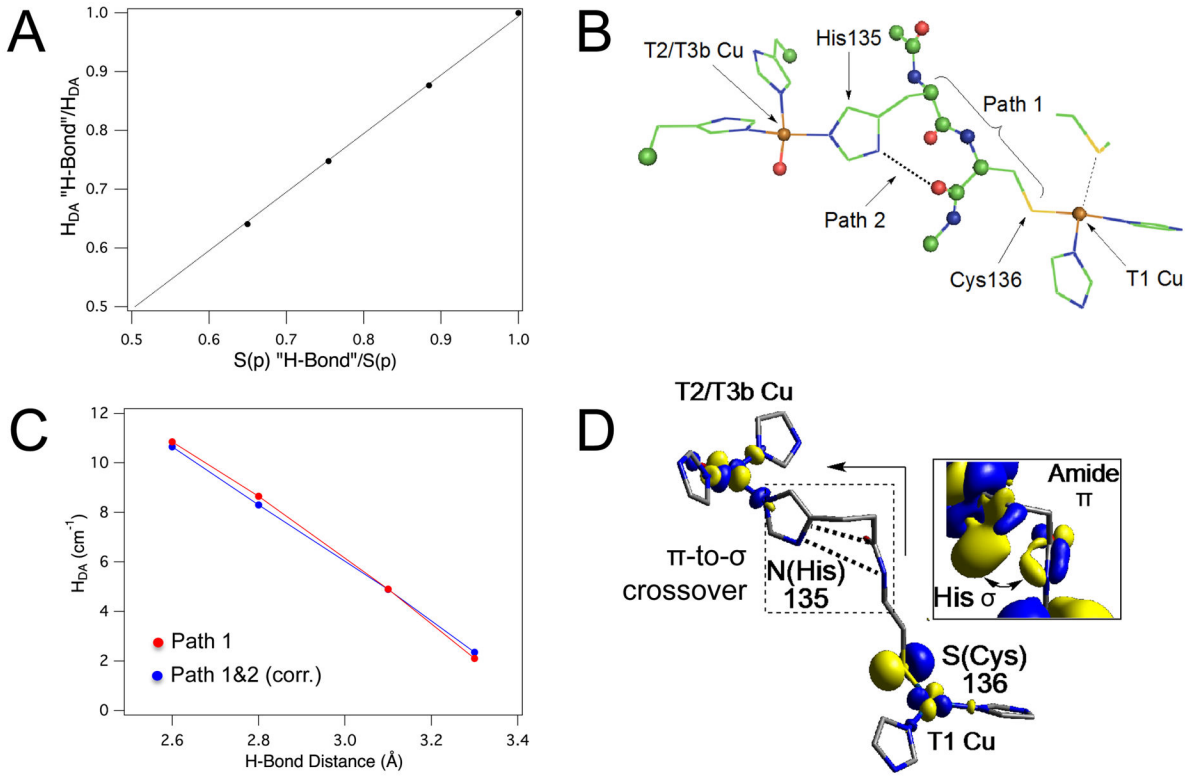

Figure 9.

Electronic structure contributions to intramolecular electron transfer within a multi-copper oxidase. (A) Linear relationship between Cu-S covalency and H_{DA} (both normalized to their maximal values). (B) Structure of Cys-His link, showing two superexchange pathways. (C) Influence of H-bond (dotted line in (B)) on H_{DA} through the Cys-His link, demonstrating the dominant contribution of path 1. (D) Molecular orbital interactions mediating superexchange through the Cys-His link. Insert gives detail of the π to σ crossover (see [22] for details). Adapted with permission from [22]. Copyright 2014, American Chemical Society.

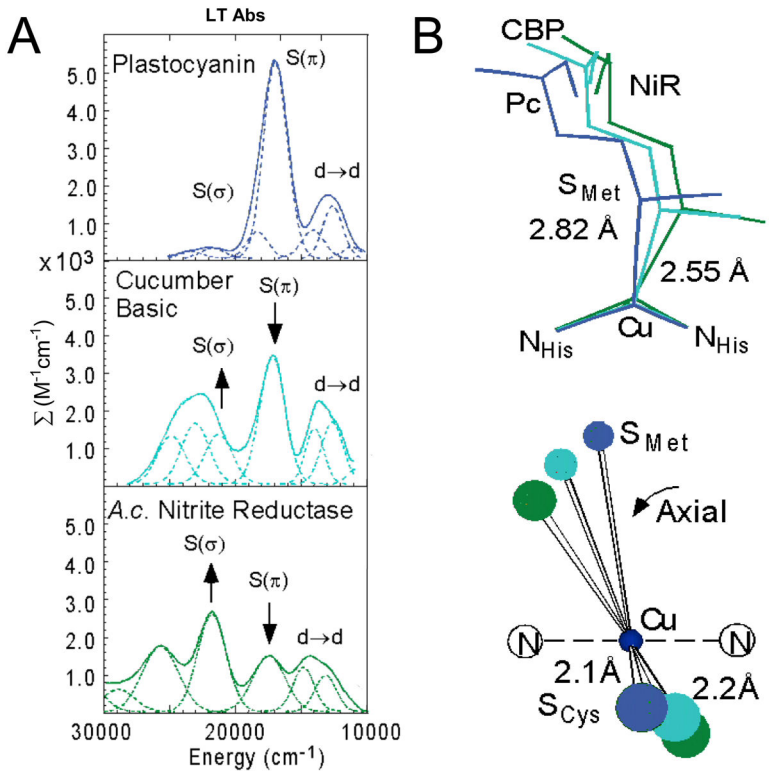

Figure 10.

Correlation of (A) Abs features and (B) geometric structures of a series of sites related to blue Cu with Cys, Met, and 2His ligation. Adapted with permission from [23a]. Copyright 1998, American Chemical Society.

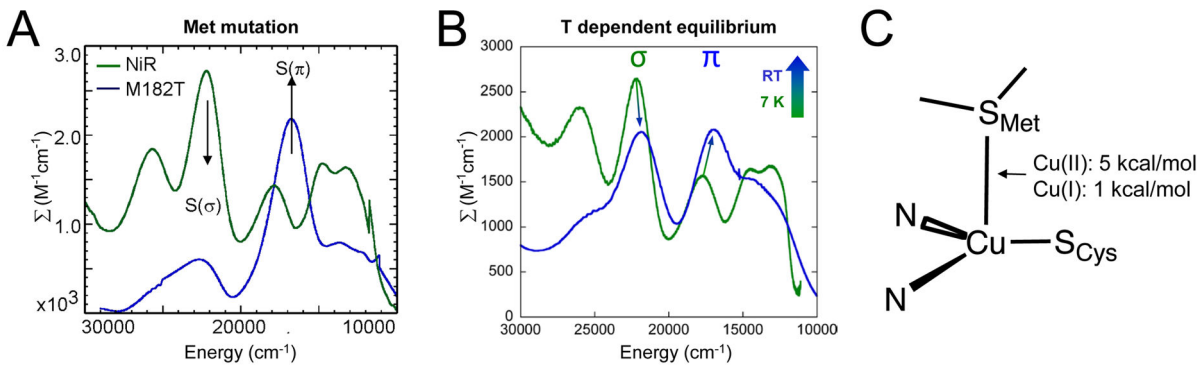

Figure 11.

(A) Comparison of Abs data from wild-type NiR (green) and NiR lacking axial thioether ligation from M182 (blue). (B) Thermodynamic equilibrium between green and blue Cu sites in NiR. (C) Estimates of the Cu-S_{Met} bond enthalpies.

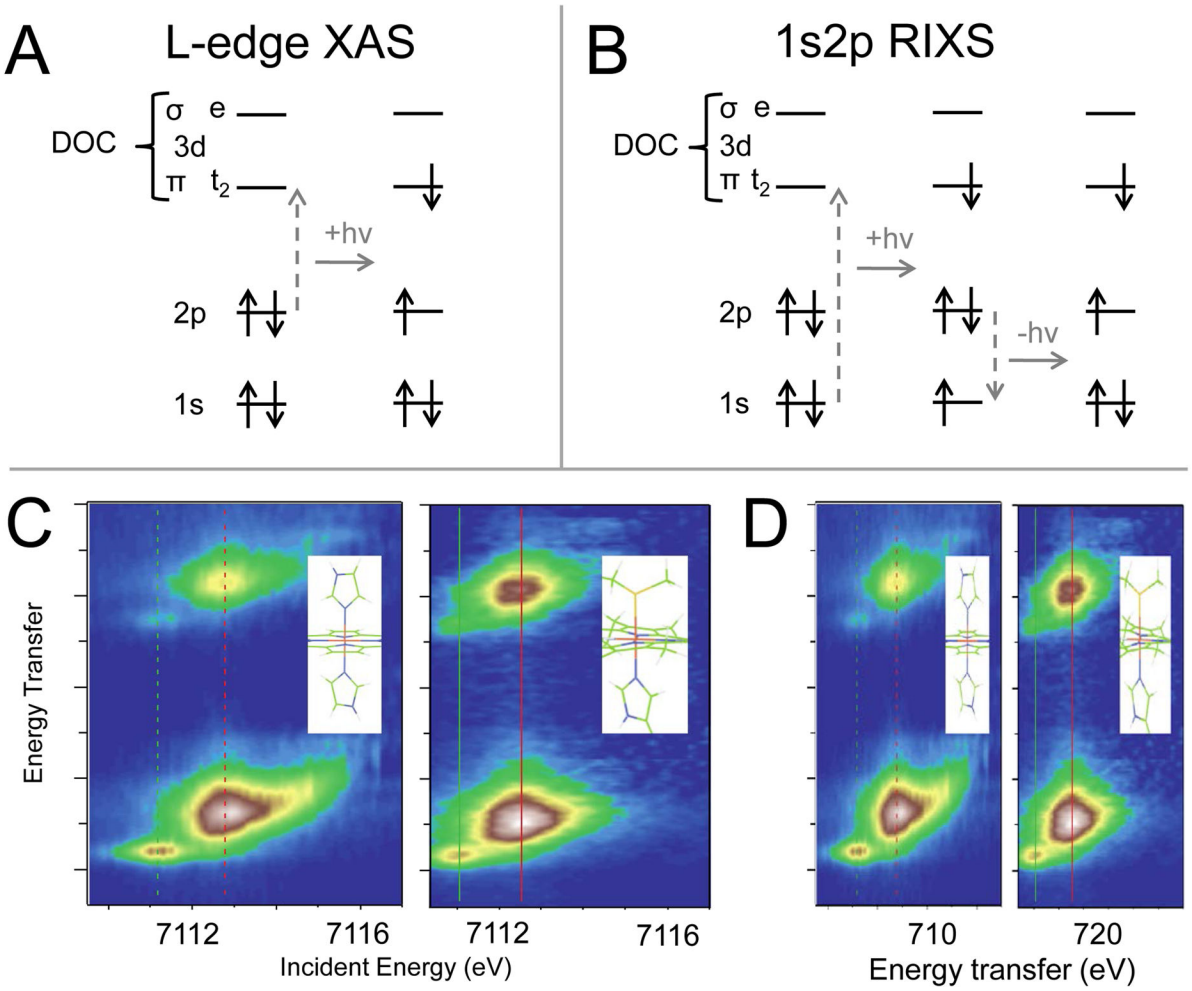

Figure 12.

(A) The 2p→3d transition in L-edge XAS. (B) The coupled 1s→3d excitation and 2p→1s emission in 1s2p RIXS. (C) 1s2p RIXS planes from low spin ferric cyt *c* (right) and a low spin bis-imidazole Fe(III) reference compound (left). (D) Constant incident energy cuts ("L-edge like" spectra) taken from RIXS planes indicated by vertical lines in (C). Adapted with permission from [28]. Copyright 2014, American Chemical Society.

Table 1

Comparison of experimental (XAS, green row) and DFT-calculated covalency of the Cu-S_{cys} bond (white rows – small model, yellow rows – larger model). Adapted with permission from [1b]. Copyright 2006, American Chemical Society.

model	functional	atomic spin density	
		Cu	S_{Cys}
33-atom QM	BP86	0.27	0.61
	B3LYP	0.33	0.57
experiment (XAS)		0.41 d	0.38 p
217-atom QM (includes protein dipoles and H-bond to S_{Cys})	B3LYP	0.43	0.43
QM/MM, all protein	B3LYP	0.44	0.42

Table 2

DFT-calculated Fe-S_{Met}, Fe-N_{His}, and Fe-OH_2 bond strengths for cyt *c*. ΔΔH indicates the change in enthalpy of the metal-ligand bond between the Fe^{II} and Fe^{III} states.

	Fe^{II}-S_{Met}	**Fe^{III}-S_{Met}**	**ΔΔH S_{Met}**	**Fe^{II}-N_{His}**	**Fe^{III}-N_{His}**	**ΔΔH N_{His}**	**ΔΔH O(H_2O)**
ΔH (kcal/mol)	2.6	5.5	2.9	7.2	14.7	7.5	7.3